Wiley
International Journal of Energy Research
Volume 2024, Article ID 4425634, 15 pages
https://doi.org/10.1155/2024/4425634

WILEY

Research Article

CFD Modeling of a Pitching Airfoil for the Estimation of the Performance Curve in an H-Rotor Vertical Axis Wind Turbine

Luis Santamaria, Jesús M. Fernández Oro, Pedro García-Regodeseves, Sandra Velarde-Suárez, and Adrián Pandal

Área de Mecánica de Fluidos (EDZE), Campus de Viesques, Universidad de Oviedo, Gijón 33203, Asturias, Spain

Correspondence should be addressed to Adrián Pandal; pandaladrian@uniovi.es

Received 24 April 2024; Accepted 3 July 2024

Academic Editor: Payman Jalali

In this work, the performance curve of a straight-bladed vertical axis wind turbine (VAWT) is estimated through a CFD two-dimensional modeling of a single airfoil under unsteady pitching motion. A typical URANS approach, with a k-ω SST turbulence model and UDF functionalities, has been employed to simulate a fixed airfoil under variable inlet conditions. Induction factors are previously computed using a simple stream tube model (SSTM) in an iterative process. Frequencies and amplitudes of the pitching motion are modified to simulate the operative range of tip-speed ratios (TSRs) for the wind turbine. The obtained results have been compared with experimental curves of a 0.5 solidity turbine measured in a wind tunnel. The experimental results of the wind-tunnel turbine provide a maximum C_p value of 0.22 at a TSR = 3.1, while the numerical procedure estimates a value of 0.33, also at TSR = 3.1. Despite of the discrepancy, due to the 2D assumptions in the simulation, the procedure makes reliable and more accurate estimations than traditional analytical models with steady coefficients. This alternative methodology significantly reduces the computational cost. Moreover, these nonrotating simulations allow more robust and practical routines that can be easily implemented in optimization algorithms for the design of VAWTs.

1. Introduction

Remarkable objectives have been set for decarbonization with special focus on sustainable and affordable energy. Among renewable technologies to tackle these objectives, wind energy is one of the leading ones, with high level of maturity and good profitability as main advantages. However, conventional wind technologies, i.e., horizontal axis wind turbines (HAWT), are not well-suited for challenging applications such as deepwater offshore installations, urban environments, or self-consumption in remote locations. Instead, favored by the improvements in electrical supply chains, lift-type vertical axis wind turbines (VAWT) have emerged as good candidates for this purpose [1, 2]. VAWT have interesting advantages such as omnidirectionality, reduced noise, lower gravity center, and are better suited for wind farms, even exhibiting synergic behaviors in some configurations [3, 4, 5]. Nevertheless, their highly complex aerodynamics due to cross-flow have been a strong impediment to their development.

More precisely, the blades of a vertical-axis wind turbine experience a continuous variation of the incoming incident flow angle and its associated Reynolds number as a function of its azimuthal rotation. In the case of H-rotor straight blades, this variation is equivalent to a pitching motion of an aerodynamic airfoil in a cascade environment, either linear (if the chord-diameter ratio is sufficiently reduced) or rotational (if considering the rigid body motion of the blades in the absolute frame for a general case).

Actuator disk approaches along with blade element method (BEM) are typically combined to pose analytical models that may estimate the performance curve of a VAWT design within few minutes of CPU time. However, they require appropriate values of the lift and drag coefficients, which are practically nonavailable in the case of dynamic conditions and massive separation (dynamic stall). To improve those estimations, additional corrections are also introduced to consider three-dimensional effects (tip and strut losses and/or curvature

effects), but the application of static aerodynamic coefficients is still the major issue to deal with.

On the other hand, computational fluid dynamics (CFD) simulations of a complete 3D VAWT have huge computational costs due to turbulence modeling [6], 3D mesh generation, and motion simulation. Hence, the range of studied geometries is usually limited.

In this work, a hybrid approach is evaluated. This hybrid approach reduces the complexity and computational costs of VAWT CFD simulations by modeling a single airfoil under unsteady pitching motion. Meanwhile, to consider the "macro" effect of the turbine in the flow perceived by the airfoil, appropriate induction factors are introduced using analytical models. Then, both analytical models and CFD simulations feed each other in an iterative manner, in the search of convergence to a more realistic solution.

This process is detailed throughout the paper with the following structure. First, the studied VAWT turbine characteristics are stated, as well as the previous works from where reference data have been obtained. Next, the applied analytical models are described and the prescribed relationship with the boundary conditions for the simulations is formally derived. Then, the CFD mesh and models are explained in detail, presenting two different methodologies, linear and rotating cascade. Afterward, the initial results and iterative routine are shown, giving way to the final iterated results. Finally, conclusions about the developed methodology are posed, identifying critical areas, and proposing future works.

2. Materials and Methods

In this section, the prototype of the vertical-axis wind turbine is presented, and the different analytical and numerical methodologies are described in detail.

2.1. Geometry of the H-Rotor VAWT Prototype. The authors have recently designed a three-bladed vertical axis wind turbine (VAWT) with an H-rotor design based on the DU 06-W-200 profile. This innovative model, designed explicitly for urban settings as outlined by Kumar et al. [2], boasts reduced manufacturing expenses compared to alternative VAWT architectures, while delivering commendable efficiency [7].

Following, a small-scale prototype has been built for wind tunnel testing with a diameter of 0.8 m and equipped with three blades, each measuring 0.067 m in chord length and spanning 0.6 m [8]. This configuration yields an aspect ratio of $H/D = 0.75$ and a solidity of $\sigma = 0.5$. Struts are covered with an Eppler 863 airfoil to further reduce drag forces. Table 1 provides a concise summary of the key geometrical characteristics, which are in concordance with recommended values in the literature for VAWT designs [9].

2.2. Experimental Characterization of the VAWT. The characterization of the aerodynamic performance of the turbine was determined in a wind tunnel, 24.6 m in total length, and operated in a closed-loop layout employing a 30 kW axial fan. The aerodynamic test section measures $1.05 \times 1.25\ m^2$ and is immersed in a 4.2 m long anechoic chamber. Speeds up to 22 m/s can be reached, corresponding to maximum Reynolds number of 1.7×10^6 (based on the nozzle hydraulic diameter), maintaining a mean turbulence intensity of approximately 0.7%.

Table 1: Main dimensions of the VAWT prototype.

Blade airfoil	DU 06-W-200
Blade number (N)	3
Blade chord (c)	0.067 m
Diameter (D)	0.8 m
Blade span (H)	0.6 m
Solidity ($\sigma = 2Nc/D$)	0.5
Aspect ratio (H/D)	0.75
Struts airfoil	Eppler 863

Figure 1: Aerodynamic enclosure with the turbine in the wind tunnel.

For the current study, a hybrid modular enclosure has been employed to establish a semiconfined environment without wake blockage. This enclosure is extended for 1.7 m downstream of the wind tunnel nozzle, so the stream tube is preserved constant along the turbine. Otherwise, at high TSRs (typically higher than 2.7 for this turbine), the axial blockage of the turbine diverts the flow outside of the turbine, so the flow inlet is no longer uniform. The blockage ratio generated is additionally corrected using the correlations proposed by Jeong et al. [10] in order to obtain extrapolatable values for open-field conditions. Figure 1 illustrates the turbine positioned within the enclosure in the wind tunnel's test chamber.

The performance curve of the VAWT has been obtained experimentally using a methodology based on an active driving mode (ADM) operation of the turbine. ADM is based on the reproduction of the same kinematic conditions that are established in the turbine when it is wind-driven operated. To do so, the torque in the turbine is increased by an external motor that fixes the rotating speed to assure the required TSR. The developed methodology, which is described in detail in Santamaría et al. [8], employs a precise subtraction of the system losses so the aerodynamic power in the turbine can be finally isolated. This alternative avoids the common constraints encountered in prototypes of smaller dimensions when utilizing conventional passive driving modes to measure power. These constraints include issues related to self-starting, cut-in thresholds, excessive frictional losses, and limited operational ranges [11, 12, 13].

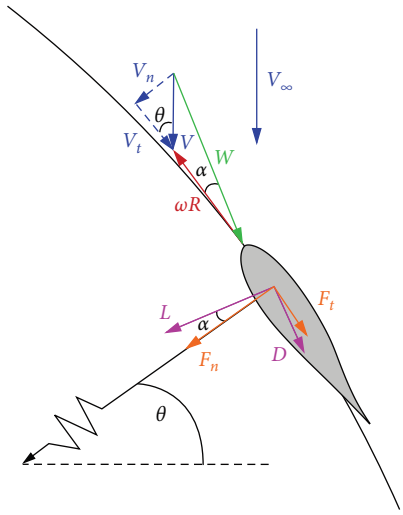

FIGURE 2: Sketch of drag and lift coefficients.

2.3. Analytical Models and Prediction of the Performance Curve. While CFD and experimental approaches are valuable for VAWT characterization, current analytical models emerge as the most practical method for rapid estimation of performance and optimization tasks. These models typically provide the variation of the power coefficient, C_p, of the turbine as a function of the tip-speed ratio (TSR), λ, following the well-known definitions:

$$C_p = \frac{P}{\frac{1}{2}\rho V_\infty^3 DH}, \tag{1}$$

$$\lambda = \frac{\omega D}{2V_0}, \tag{2}$$

where P is the aerodynamic power, r is the air density, V_∞ is the wind velocity, D and H are the diameter and span of the turbine, respectively, and w is the rotational speed. Classic bibliography proposes three different analytical models based on stream-tube modeling and blade element theory: (1) the single stream tube model (SSTM), proposed by Templin; (2) the multiple stream tube model (MSTM); (3) and the double disk multiple stream tube model (DMST) [14]. Typical computation time for each model in MATLAB coding is lower than 5 min. Figure 2 shows a sketch used in the SSTM model for the calculation of drag and lift coefficients, with the kinematic conditions of the blades as a function of their azimuthal position during the turbine rotation. The effective velocity (V) over the blade is reduced from the incoming flow (V) by the induction factor (a) that considers the blockage effect of the turbine (Equation (3)). For this simplified model, a single value of the induction factor is considered representative for the whole disk:

$$V = V_\infty(1 - a). \tag{3}$$

According to the forces in the figure, the instantaneous power given by a single blade at a particular angular coordinate is obtained as follows:

$$P(\theta) = \frac{1}{2}\rho W^2 cH\omega R(C_L \cdot \sin\alpha - C_D \cdot \cos\alpha), \tag{4}$$

where

$$\alpha = a\tan\left[\frac{(1-a)\sin\theta}{\lambda + (1-a)\cos\theta}\right], \tag{5}$$

$$W = V_\infty\sqrt{(1-a)^2 + 2\lambda(1-a)\cos\theta + \lambda^2}, \tag{6}$$

where W is the relative velocity, c is the blade chord, C_D and C_L are the drag and lift coefficients, respectively, and a is the angle-of-attack (AoA). Computing the integrated value for a whole revolution of the blade and for the total number of blades, the averaged value of power as a function of the TSR is obtained. Note that the major problem of analytical models is the requirement of accurate values of drag and lift coefficients as a function of the AoA and blade Reynolds number. The typical approach is the employment of 2D static aerodynamic coefficients in a linear cascade configuration, in which a certain angle of attack is set for the incident current and the static forces on the airfoil are determined. Once stabilized, the AoA is modified, repeating the procedure as many times as the angular range of interest has been predefined. In this way, "static" aerodynamic coefficients are generally obtained, valid for stationary incident flow situations. These coefficients can be obtained experimentally or numerically. However, literature does not provide sufficient experimental data, especially for high angles of attack and low Reynolds numbers, so numerical data from 1D codes, like XFOIL or JavaFoil, is used in most cases.

A significant improvement can be fulfilled by obtaining the drag and lift coefficients using CFD-based numerical simulations, where well-adapted turbulence models predict the airfoil performance more accurately. A compromise between simulation time and results must be preserved, focusing on the prediction of aerodynamic forces rather than in flow field characteristics. Several models based on unsteady reynolds-averaging of the Navier–Stokes equation (URANS) as well as simulations with turbulent Scale Resolution (SRS), such as scale adaptive simulation (SAS) or even DES simulations can be used. In the authors' experience, turbulence models based on k-ω provided the most accurate predictions of aerodynamic forces for reasonable CPU time.

Figure 3 shows the aerodynamic coefficients of the DU-06-W-200 profile used for the turbine. Both numerical and experimental results were obtained at $\mathrm{Re} = 2 \times 10^5$ using the typical static, linear cascade methodology for angles-of-attack between −20° and 20°. Numerical results were calculated using a 2D URANS modeling with the generalized k-ω turbulence (GEKO) model and SAS option activated. The experimental results, measured using an external, three-component strain-gauge balance, allowed the validation of the numerical model [15], which was further employed to obtain lift and drag coefficients for a significant

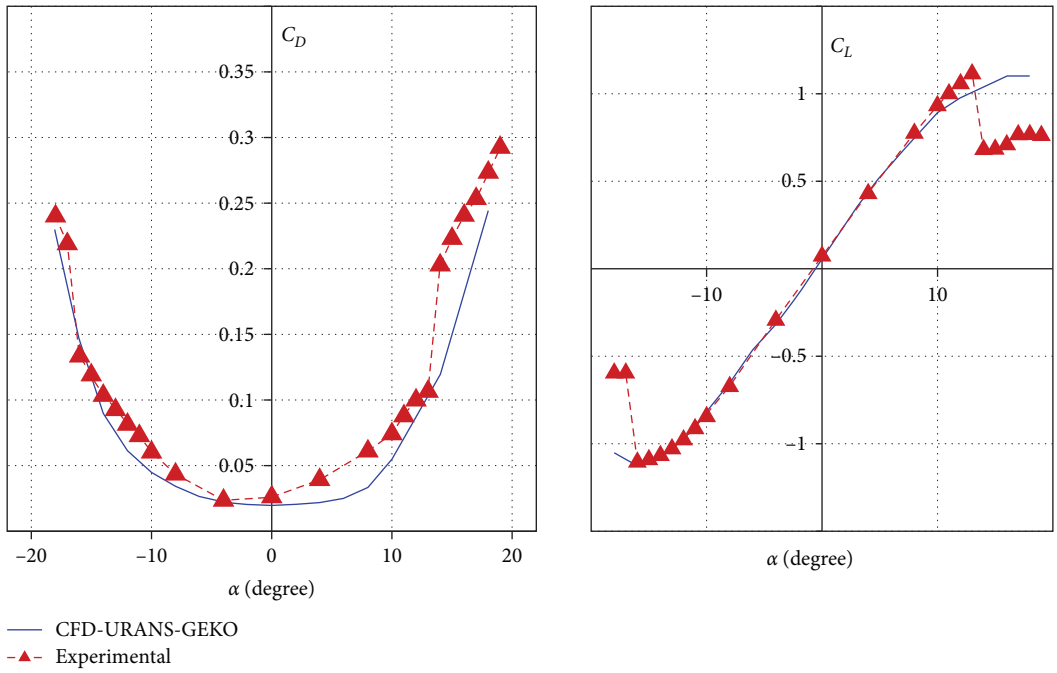

FIGURE 3: Aerodynamic coefficients of the DU-06-W-200 airfoil in linear, static cascade. Comparison between experiments and numerical results at $\mathrm{Re} = 2 \times 10^5$.

range of Reynolds numbers (between 5×10^4 and 3×10^5). Finally, this dataset was employed in the analytical model to calculate the performance curve of the turbine using Equations (4), (5), and (6).

This combination of analytical models and aerodynamic coefficients from static linear cascades takes into account the variation of the angle of attack and the relative velocity with the azimuthal angle of the turbine, as well as the induction factor. However, they neglect the dynamic effects associated to fast and periodic changes in the angle of attack and even in the corresponding Reynolds number. Hence, these aerodynamic coefficients are not totally representative of the forces experienced by the blades in the VAWT environment.

To overcome this issue, a CFD-based numerical simulation of the 2D airfoil in a pitching motion is developed in this work, so more realistic estimations of the aerodynamic coefficients are obtained, reproducing with more fidelity the flow characteristics of the turbine.

2.4. Lift and Drag Coefficients in Pitching Motion. More accurate aerodynamic coefficients are expected through a numerical simulation of the flow around the airfoil under pitching airfoil conditions. By analyzing how the AoA of the flow over the airfoil changes as it rotates in the turbine (function of the TSR), an equivalent situation of a single blade oscillating (pitching) at a frequency and amplitude similar to the law of variation of the AoA over the rotating airfoil of the VAWT turbine can be considered.

Typically, a "reduced frequency" k is defined as the comparison between the time it takes for the blade to make one complete pitching cycle (i.e., covering the whole set of AoA for one revolution) and the throughflow time (Equation (7)). Meanwhile, an "equivalent amplitude" is set as the difference between the maximum and minimum values of AoA, according to Equation (8). Additionally, the induction effect perceived by the airfoil as it is immersed in the turbine disk must be imposed. This results in an effective decrease of the incident wind speed. Moreover, this feature complicates the whole process because the induction factor is not known a priori, thus requiring the employment of an iterative process. The initial guess of the induction factor can be obtained from the analytical models themselves solved with the static coefficients known from the literature or from previous tests (numerical or experimental). When introducing the induction factor a, the following equations are yielded:

$$\kappa = \lambda\sigma/N, \tag{7}$$

$$\alpha = a\tan\left[\frac{(1-a)\sin\left(\frac{V_\infty \kappa t}{c}\right)}{\lambda + (1-a)\cos\left(\frac{V_\infty \kappa t}{c}\right)}\right], \tag{8}$$

where the reduced frequency depends on the TSR, the solidity σ, and the number of blades N. The velocity relative to the airfoil (W) is also modified with the angular position (azimuthal position of the turbine rotation: $\theta = V_\infty \kappa t/c$), function of time t, and must be varied in the simulation input according to the following equation:

$$W = V_\infty \sqrt{(1-a)^2 + 2\lambda(1-a)\cos\left(\frac{V_\infty \kappa t}{c}\right) + \lambda^2}. \tag{9}$$

From Equations (8) and (9), which define the relative inlet velocity and its angle, both chordwise and perpendicular components can be directly introduced as boundary

conditions for the UDF utility. This is simply expressed as follows:

$$W_t = W\cos\alpha, \tag{10}$$

$$W_n = W\sin\alpha. \tag{11}$$

Although in a first approximation, the simulation of the "pitching" of the airfoil can be performed assuming linear cascade flow, the airfoil wakes are clearly helical, which implies a clear effect of the rotational force on the boundary layer structure and the generation of turbulence in the blades. It is even possible to go a step further and perform the simulation of the pitching behavior considering that the airfoil is also subject to a rotational motion. Thus, depending on the values of turbine solidity and radius, it is more appropriate to simulate assuming that the blade under pitching AoA also follows a circumferential trajectory. For this purpose, it is sufficient to incorporate, into the absolute frame, the rotational speed of the rotating domain for the blade. In this case, the inlet velocity for the boundary condition must be the absolute velocity (reduced by induction effects), instead of the relative W in Equation (9), which can be further decomposed into tangential (or chordwise) and perpendicular components to the blade by means of the azimuthal angle of the airfoil. Hence, the inlet velocity components to be introduced in the simulation should be as follows:

$$V_t = V_\infty(1-a)\cos\left(\frac{V_\infty \kappa t}{c}\right), \tag{12}$$

$$V_n = V_\infty(1-a)\sin\left(\frac{V_\infty \kappa t}{c}\right). \tag{13}$$

In addition, the airfoil performance for every TSR simulation must be completed by modifying the corresponding value of the rotational speed in the absolute domain: $\omega = \lambda V_\infty / R$.

2.5. Numerical CFD Modeling of the Pitching Motion. An implementation of a 2D numerical model for the DU-06-W-200 airfoil was conducted using Ansys-FLUENT®2023 to numerically derive aerodynamic coefficients. The resolution of the unsteady Reynolds-averaged Navier–Stokes (URANS) equations was carried out through an incompressible approach employing eddy–viscosity turbulence modeling. The widely applied one-equation Spalart–Allmaras model [16] is commonly employed in external aerodynamic applications for airfoil characterization. While acknowledged for providing reasonable solutions in flows with adverse pressure gradients and separation, its accuracy in predicting separation is inferior to optimal two-equation models such as k-ω omega SST and GEKO. Additionally, all k-ω models in ANSYS incorporate a y+-insensitive wall treatment, eliminating the need for discussions regarding the optimal selection of wall formulations in k-ε models [17].

GEKO represents a recent turbulence model framework, utilizing the ω-equation and incorporating free parameters into the equations. The key tuning parameter for the GEKO model is the coefficient C_{SEP}, governing boundary layer separation. Increasing its value predicts a more pronounced detachment. For airfoils, a recommended range for this coefficient is between 2.0 and 2.5 [18]. Additionally, the GEKO model has been implemented with the option for SAS activated. This feature employs an enhanced URANS formulation to resolve the turbulent spectrum in unstable flow conditions.

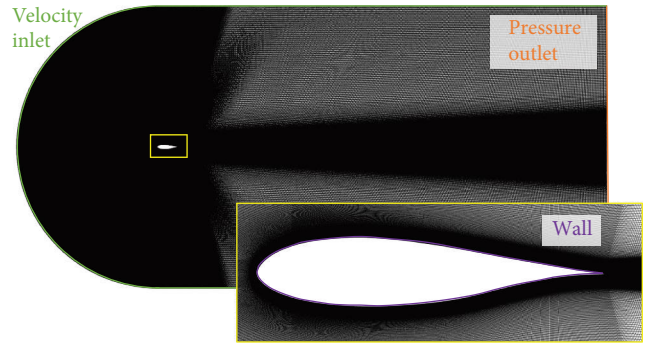

FIGURE 4: Detailed view of the CFD mesh and adopted boundary conditions.

The finite volume method with a second-order scheme was employed to discretize the flow equations, including momentum and turbulent variables. Second-order accuracy was also chosen for the transport equation governing pressure correction. Temporal terms, when necessary, were discretized using a bounded second-order implicit formulation. The pressure–velocity coupling in all cases was handled using the SIMPLEC algorithm. Spatial discretization for gradient terms utilized a least-squares cell-based approach. Convergence criteria were set at 10^{-6} for velocity components in the momentum equation, while a minimum threshold of 10^{-5} was deemed necessary for the remaining equations. Simulations were conducted on a four-node Intel Core i7-52820K at 3.3 GHz with 64 GB RAM.

An extended domain was implemented, with a distance of 12.5c from the inlet and 20c from the outlet, resulting in a domain size of 32.5c × 25c, consistent with typical values in the literature. This extended domain was carefully chosen to ensure accuracy by minimizing the impact of boundaries on the flow development within the domain region. A C-mesh distribution was applied around the airfoil, yielding a cell size of (600 × 100) for both pressure and suction sides of the airfoil. The normal 100-node meshing was progressively distributed over a 3-mm width expected for the inner side of the boundary layer. Achieving an averaged value of y+ = 0.2 (at $Re_c = 30{,}000$), the initial mesh point was positioned approximately 0.003 mm from the wall, while in the chordwise direction, an average $\Delta x = 0.1$ mm was adopted along the blade. Finally, an enhanced mesh with 475,000 cells for the entire domain was utilized to assess solution sensitivity to grid resolution. The boundary conditions of the simulation domain are given in Figure 4, which includes details of the adopted mesh.

Table 2: Initial guesses of the induction factor.

λ	1.50	2.00	2.50	2.75	3.00	3.25	3.50	4.00
a_0	0.113	0.169	0.337	0.415	0.466	0.506	0.536	0.581

Table 3: Simulation time-steps for 1° resolution.

λ	1.50	2.00	2.50	2.75	3.00	3.25	3.50	4.00
T (s)	0.2234	0.1675	0.1340	0.1218	0.1117	0.1031	0.0957	0.0837
$\Delta t \times 10^{-4}$ (s)	6.2056	4.6542	3.7233	3.3848	3.1028	2.8641	2.6595	2.3271

Table 4: Working parameters for LPC database.

λ	1.50	2.00	2.50	2.75	3.00	3.25	3.50	4.00
κ	0.25	0.3333	0.4166	0.4583	0.50	0.5416	0.5833	0.6666

2.5.1. Initialization. All the cases are initialized resolving the steady flow for an initial velocity inlet of 7.5 m/s (assumed $a = 0$) at AoA = 0°. Following, this initial flow solution is used as the starting point to run the pitching motion, for the VAWT-like environment, using a UDF to modify unsteadily the inlet velocity according to previous equations, as shown in Section 2.4.

Initial guesses of the induction factor (denoted as a_0 in Table 2) were obtained from the SSTM analytical model, executed for eight different values of the TSR, and using the static aerodynamic coefficients, as shown in Figure 3 (interpolating when necessary). To reach convergence of the analytical model, an under-relaxation factor of 0.2 was necessary, as well as a correction for the typical expression relating the nondimensional disk thrust with the induction factor: $C_F = 4a(1-a)^2$. In particular, it was replaced by the polynomic correction proposed by Sanvito et al. [19] to avoid the breakdown of the momentum theory due to the turbulent wake state at high induction factors:

$$a = 0.179C_F^5 - 0.9223C_F^4 + 1.6107C_F^3 - 0.8955C_F^2 + 0.4468C_F - 0.0076. \quad (14)$$

2.5.2. Unsteady Parameters. It is evident that the simulation of the pitching motion requires an unsteady flow resolution. To do so, a convenient time-step describing the alternative conditions of the incoming flow with respect to the blade must be fixed. According to Rezaeiha et al. [6], in a complete turbine simulation, a time-step equivalent to the advancement of 1° in the blade rotation of the turbine is required for a good description of the complex flow physics on the blades' boundary layer. In addition, 10–20 rotor turns are necessary for achieving a periodic-state solution of the VAWT torque. Following these guidelines, the suitable time-step for the pitching motion must be 1/360 of its cycle period, $T = 2\pi c/V_\infty \kappa$. Hence, the time-step is different for every TSR. Table 3 provides the period T of the pitching motion for every TSR and the corresponding time-step in tenths of milliseconds.

Every simulated case was executed for 10 pitching cycles, requiring approximately 2.5 hr of CPU time for each single cycle. Hence, to obtain the temporal description of the periodic-state for both lift and drag coefficients of the turbine at a given TSR value, 1 day of computations was required.

Up to this point, all the values and procedures in this section are valid for both linear and rotating pitching cascades. Following, two sets of numerical simulations were performed, introducing different operational parameters for linear and rotating pitching motions.

2.5.3. Parameters for Linear Pitching Cascade (LPC). Using the reference case as a starting point, a UDF was implemented for the velocity-inlet boundary condition to implement the *velocity components in the relative frame* according to Equations (10) and (11). Note that, according to these equations, the blade is static and the pitching motion is produced changing the magnitudes of the two components of the inlet relative flow.

For the eight different TSRs tested, the following values of the reduced frequency (Equation (7))—summarized in Table 4—were also introduced in the UDF of every simulation.

2.5.4. Parameters for Rotating Pitching Cascade (RPC). To mimic the rotation of the blade around the turbine axis, a rotating point is introduced in the domain, at a vertical distance of 0.4 m from the connecting point of the blades to the struts of the turbine. Since the origin of coordinates of the CFD model was placed in the chord line of the blade, the 0.4 m distance is introduced, corresponding to the turbine radius, to maintain the toe-out orientation of the airfoil in the turbine. In addition, giving a corresponding value of the clockwise rotational speed for the rigid body rotation of the blade (Table 5), the pitching motion is established in a rotating fashion. In this case, working in the fixed domain, *the velocity components of the absolute incoming flow*, according to Equations (12) and (13) are then introduced in the UDF.

Table 5: Working parameters for RPC database.

λ	1.50	2.00	2.50	2.75	3.00	3.25	3.50	4.00
ω (rad/s)	28.125	37.5	46.875	51.562	56.25	60.937	65.625	75.0

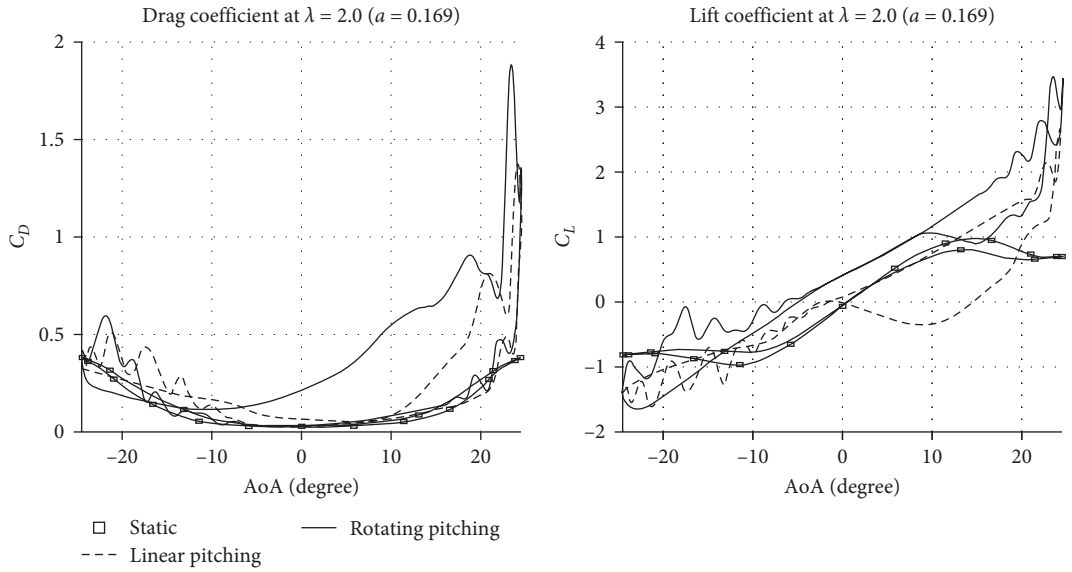

Figure 5: Comparison of drag and lift coefficients between static cascade and linear and rotating pitching cascades for low TSR ($\lambda = 2.0$).

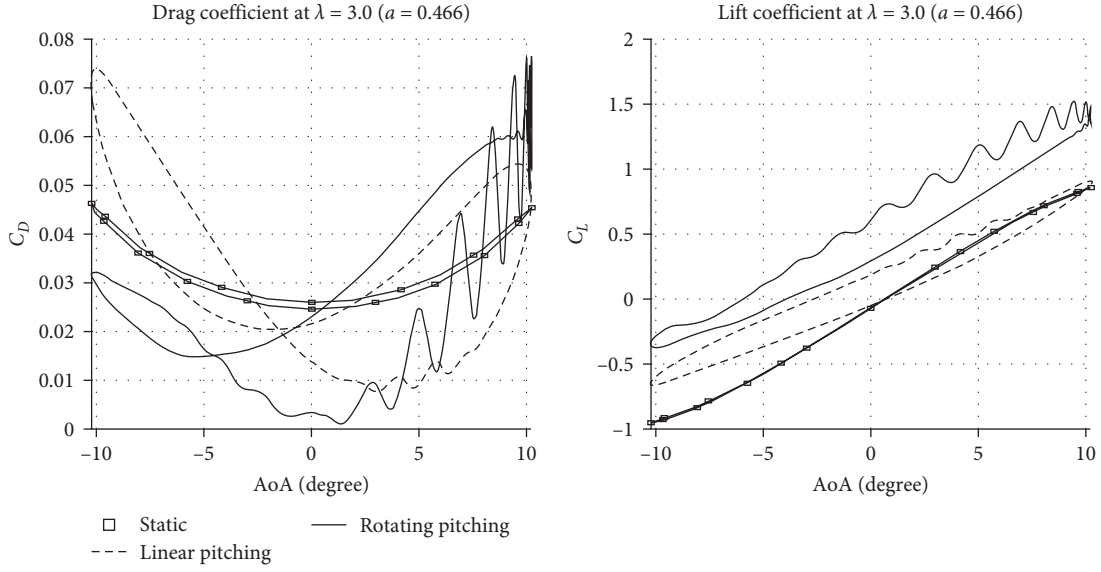

Figure 6: Comparison of drag and lift coefficients between static cascade and linear and rotating pitching cascades for medium TSR ($\lambda = 3.0$).

3. Results and Discussion

3.1. Initial Results and Iterative Routine. Figures 5, 6, and 7 show the comparative results obtained between drag and lift coefficients through 2D CFD simulations, with a generalized k-ω (GEKO) turbulence models when using a static model of cascade flow or simulating the pitching of the airfoil, both in LPC or in RPC situations. "Static" results are represented in squared gray dots in the figures, while "linear pitching" and "rotating pitching" results are shown in dashed and solid black lines, respectively. The results correspond to the simulations performed with the initial guesses of the induction factor shown in Table 2.

Figure 5 compares results of the aerodynamic coefficients for $\lambda = 2.0$ (before maximum C_p), while Figures 6 and 7 correspond to the cases of $\lambda = 3.0$ (after maximum C_p) and

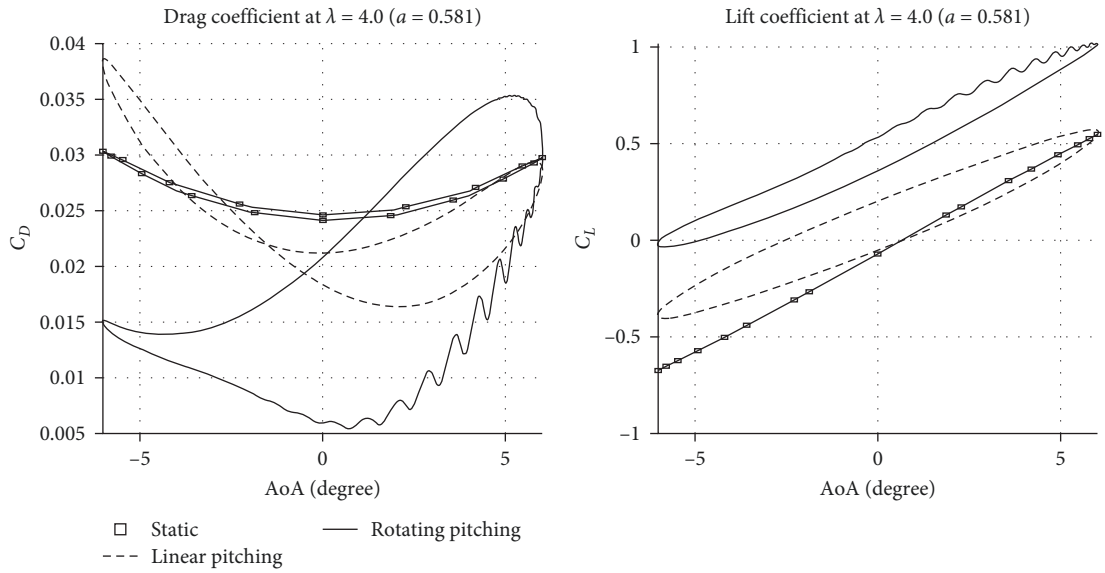

FIGURE 7: Comparison of drag and lift coefficients between static cascade and linear and rotating pitching cascades for high TSR ($\lambda = 4.0$).

TABLE 6: Reynolds range for TSR = 2.0, 3.0, and 4.0, as shown in Figure 5.

λ	2.00	3.00	4.00
Re_{min}	38,970	82,200	119,370
Re_{max}	94,370	117,800	147,300

$\lambda = 4.0$ (close to the point of no power delivery). Note in Figure 5 how the AoA range is severely decreased from $-25°$ to $25°$ at $\lambda = 2.0$ where the flow is clearly stalled for most of the AoA. In Figure 6, the values are moderate, ranging from $-10°$ to $10°$ at $\lambda = 3.0$, while in Figure 7, they are roughly between $-6°$ to $6°$ at $\lambda = 4.0$ where separation is only observed at a limited range of high AoA values. At low TSRs, the airfoil clearly suffers from vortex shedding in all cases (AoA up to 25°) but being much more pronounced in the RPC case due to the extra wake twisting effect. Even in the static case, a hysteresis cycle caused by the change in Reynolds number between the leeward and windward zones is observed (more pronounced in the lift coefficient). Moreover, not only these severe changes in the AoA play a significant role in the aerodynamic coefficients. Reynolds numbers are also highly modified, especially at low TSRs, reaching very reduced values (far below 10^5) that penalize the overall aerodynamic behavior of the blades. Table 6 summarizes the maximum and minimum values of the Reynolds number on the blades (which are attained at AoA = 0°, corresponding to equivalent positions of the blade in the turbine at $q = 0°$—windward—and $q = 180°$—leeward).

In addition, at high TSRs, angles of attack of $\pm 6°$ are not exceeded so that the profile does not perceive massive shedding (evident in the static case), although hysteresis is observed in the forces in the pitching case with some slight instabilities associated with the return flow. In any case, the rotating pitching cases always anticipate more severe detached flow conditions. These observed features and considering the relevance of the rotating wakes in the turbine blades justify the selection of the RPC database to proceed with the iterative process until the converged values of the induction factor are finally met.

The iterative process has now started introducing the RPC results in the recalculation of the performance curve with the SSTM analytical model. Since the changes in the polar data are so abrupt with respect the initial static coefficients, the iterative recalculation requires also to be relaxed, introducing a typical factor of 0.2. After three iterations, the values of the induction factor are considered sufficiently converged (Table 7). The final values employed to determine the definitive performance curve using the SSTM model are also given in the table.

Furthermore, a 2D URANS simulation of the complete confined turbine layout, previously developed by the authors for validation purposes, is revisited now to compare its basic flow features with those observed in the pitching results. Details about spatial and temporal discretization and control parameters of the simulation can be found in [8]. Contours of nondimensional vorticity over the blades of the turbine are represented for three azimuthal angular positions: $q = 90°$, 210°, and 330°. Previous results are denoted as "VAWT," while results coming from the rotating pitch approach (using the converged values of the third iteration) are superimposed at every angular position and denoted as "RPC." Figure 8 shows the comparison for TSR = 2, while Figures 9 and 10 provide the comparison for TSR = 3 and 4, respectively. Background vorticity in the figures corresponds to the VAWT results, showing the influence of the convection of adjacent wakes in the development of the singular wake of the blade. To improve the visualization, the scale has been limited to values between −4 and 4 for all the cases.

At low tip speed ratios, it is revealed how the impact of viscous mechanisms of the convected wakes significantly affects the generation of vorticity in the blades. Though massive separations developed at the angular positions of 90° and 330° are well predicted by the pitching approach, other

Table 7: Iterative values of the induction factor for the rotating pitch.

λ	1.50	2.00	2.50	2.75	3.00	3.25	3.50	4.00
First Iteration ($a_1 = 0.8a_0 + 0.2a_{1^*}$)								
a_{1^*}	0.231	0.381	0.514	0.528	0.518	0.530	0.559	0.594
a_1	0.1369	0.2124	0.3724	0.4380	0.4788	0.5110	0.5406	0.5854
Second Iteration ($a_2 = 0.8a_1 + 0.2a_{2^*}$)								
a_{2^*}	0.229	0.387	0.482	0.486	0.504	0.523	0.555	0.587
a_2	0.1553	0.2473	0.3943	0.4476	0.4838	0.5134	0.5435	0.5857
Third Iteration ($a_3 = 0.8a_2 + 0.2a_{3^*}$)								
a_{3^*}	0.213	0.392	0.473	0.466	0.496	0.518	0.553	0.581
a_3	0.1669	0.2763	0.4101	0.4513	0.4863	0.5143	0.5454	0.5848

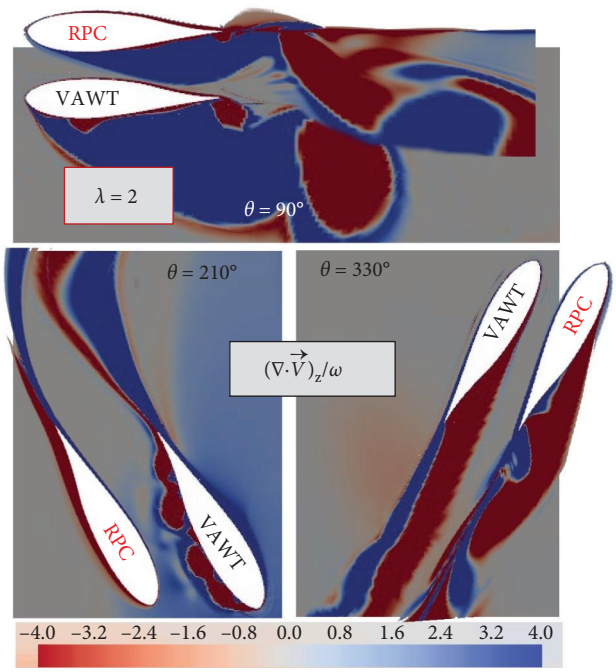

Figure 8: Nondimensional vorticity around the blades for low TSR, $\lambda = 2.0$. Comparison between a conventional 2D URANS three-bladed simulation (VAWT) and the rotating pitching approach (RPC).

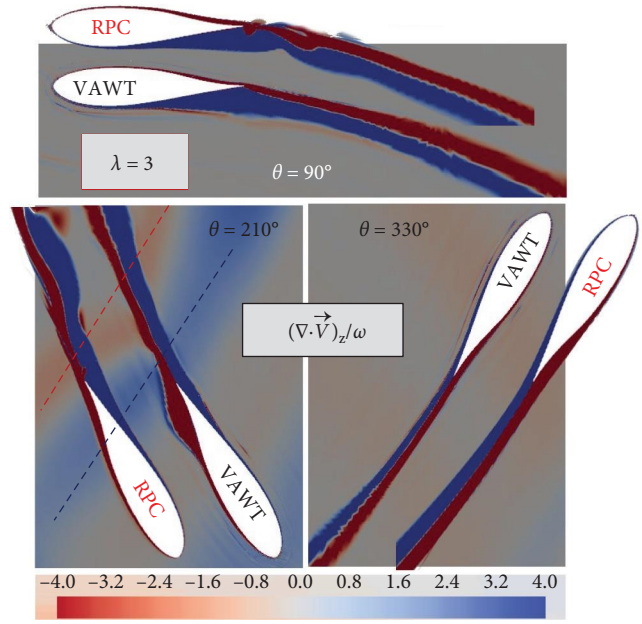

Figure 9: Nondimensional vorticity around the blades for medium TSR, $\lambda = 3.0$. Comparison between a conventional 2D URANS three-bladed simulation (VAWT) and the rotating pitching approach (RPC).

small-scale phenomena associated with the interaction of background wakes are not observed. Nevertheless, the width evolution of the blade wake at all the angular positions is reasonably well-reproduced. Moreover, at 90°, the shedding frequency of the high stalled vortex is captured by the pitching approach.

Following, in Figure 9, the results for a medium TSR close to the optimal value are presented. Note how in this case, results from both simulations predict much thinner wakes with no significant detached regions (for those angular positions shown). The curvatures of the wakes in the RPC approach also agree with those previously obtained in the conventional VAWT simulation. Only at 210°, the influence of background wakes (see dashed colored lines) significantly interacts with the outer side of the blade, engrossing the wake with negative values of vorticity. Nevertheless, the RPC approach is capable to reproduce the wake instabilities coming from the own variation of the separation point in the blades, as shown in that angular position.

Finally, Figure 10 reveals a good match between the results of the RPC approach and the previous VAWT simulation. Note especially how at 90° and 330° the wakes in both simulations are consistent and stable and with similar characteristics of width and curvature in both sides. Only at 210°, the influence of the background wakes modifies the meandering behavior of the blade wake in the VAWT case.

As expected, viscous interactions due to unmixed background wakes are more relevant at low tip-speed ratios, typically for operational points prior to the maximum power coefficient. At moderate-to-high TSR, despite of the arising of more background wakes in helical arrangement, they are notably weaker, thus being marginal for the flow over the blades and the associated forces distributions (lift and drag). Moreover, this contribution is also highly mitigated in the case of medium-to-low solidities which correspond to designs

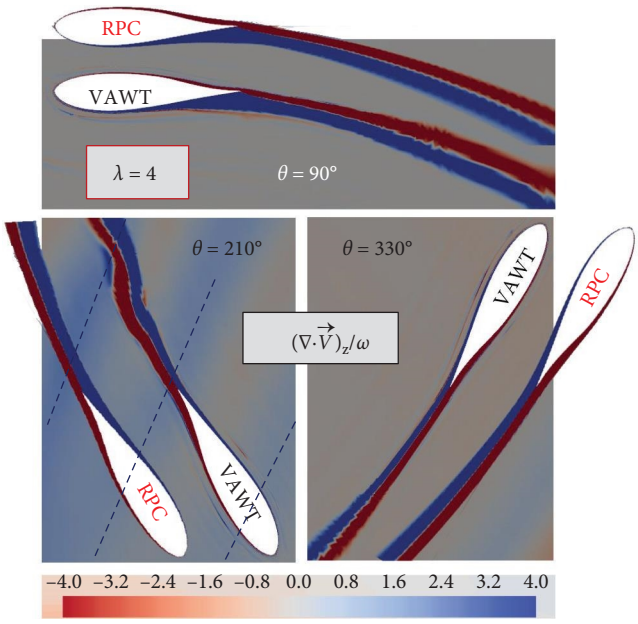

FIGURE 10: Nondimensional vorticity around the blades for high TSR, $\lambda = 4.0$. Comparison between a conventional 2D URANS three-bladed simulation (VAWT) and the rotating pitching approach (RPC).

with higher efficiencies [6], as in the situation of this turbine design.

Note that the significant advantage of the RPC simulations is derived from the computational savings gained in terms of geometry complexity, meshing, and CPU times required with respect to the full-bladed conventional VAWT simulation. Approximately, a reduction between a 30% and 80% of the total computational effort can be achieved considering the reduction of domain required, stabilization and transient times, and overall flow complexity. This justifies the employment of the RPC approach to obtain the performance curve of VAWT designs. Moreover, in the case of optimization routines, where variation of several geometrical parameters for the optimal working conditions is the objective, the simplified pitching approach provides an excellent balance between sufficient accuracy and computational cost.

In addition to previous qualitative results, the pressure coefficients over the blades for those three intermediate angular positions (90°, 210°, and 330°) have been obtained and compared for both numerical simulations. The pressure coefficients have been defined with the typical definition as $2(p - p_\infty)/\rho(\omega R)^2$, adimensionalizing with the rotational speed in each case. Note that these pressure distributions are directly linked to the final calculation of lift and drag forces on the blades. Figure 11 shows the results obtained for low TSR ($\lambda = 2.0$), where the impact of unmixed wakes was revealed significant. Red dots correspond to the results of the pitching approach while black dots were obtained from the conventional VAWT turbine. Effectively, at 210°, there are significant oscillations on the pressure coefficient on the suction side, though the overall trend of the distribution is well-captured in the pitching approach. The agreement is also quite remarkable at 330°, and even at 90° where the flow is fully detached (except for the excessively high negative values predicted in the suction side of the pitching simulation).

In Figure 12, similar evolutions of the pressure coefficients are presented, considering medium TSRs ($\lambda = 3.0$). The coincidence at 90° and 330° is again remarkable, being the position corresponding to 210° the one that is more affected by background unmixed wakes, which are not modeled in the pitching approach. Note that even in the comparisons with more discrepancies, the position of the minimum and maximum values of the pressure coefficient are always well-predicted by the pitching approach.

To conclude, Figure 13 provides similar results in the case of high TSR values ($\lambda = 4.0$), revealing again similar trends, with remarkable matches at 90° and 330°, respectively. Only the windward position at 210° exhibits higher discrepancies with notable differences in the pressure difference between both sides of the airfoil at one-fourth of the blade chord.

Having observed accurate performance of the pitching approach over local variables (wake vorticity and pressure coefficients), now the integrated results of the pitching approach are employed to estimate the global turbine performance. Hence, with the final dynamic coefficients for both drag and lift forces over the pitching airfoils, the SSTM model is finally executed to estimate the performance curve of the VAWT prototype. For completeness, the iterative process of the LPC was also performed to obtain final values of C_L and C_D coefficients (not shown here for brevity). These values were also used in the analytical models code to obtain final performance curves, as shown in Figure 14. This figure compares the results obtained with both iterative procedures (red and blue dashed lines), the static procedure (grey solid line) and the experimental one (triangular markers). Also, the numerical results of the conventional CFD simulation of the complete turbine are included (asterisks).

Both RPC and LPC cases present a less pronounced declining at high tip-speed ratios than the basic analytical model with static coefficients. Up to the maximum, their curves are practically identical, but they diverge as the effect of the rotational speed becomes more important (larger TSR values). Since the computational effort to implement RPC and LPC approaches is similar, RPC is chosen as the most convenient option. With respect to both experimental and conventional CFD results, the analytical model with static coefficient estimates the position of the maximum coefficient at lower values of the TSR. However, when aerodynamic coefficients coming from pitching simulations are used, the prediction of the TSR value for the maximum C_p is significantly improved. In particular, in the case of the rotating pitching cascade (blue line), it is practically coincident with the experimental results (triangular markers): at TSR = 3.1 for the experimental results while TSR = 3.0 for the analytical model with pitching coefficients. In addition, it is evident that the overprediction of the C_p magnitude obtained with the analytical model for the pitching approach is typical from 2D simplifications of the flow. To improve this issue, corrections accounting for 3D effects like tip losses or parasitic drag due to the struts are necessary. Moreover, the analytical

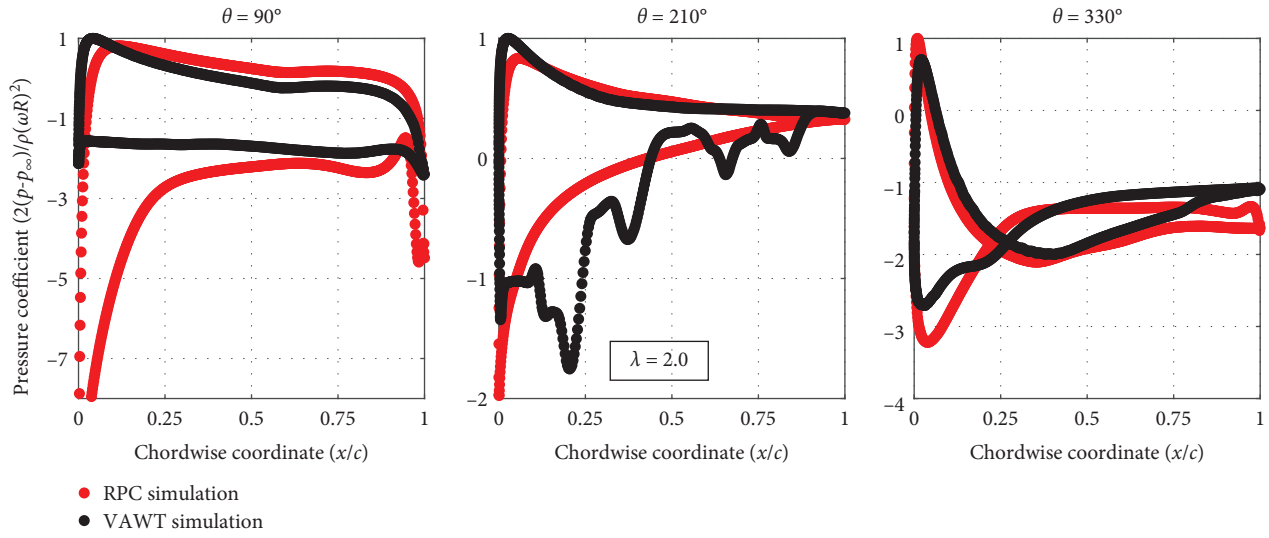

FIGURE 11: Pressure coefficients over the blades at low TSR, $\lambda = 2.0$, for azimuthal positions 90°, 210°, and 330°. Comparison between the results for a conventional 2D URANS three-bladed simulation (VAWT) and the rotating pitching approach (RPC).

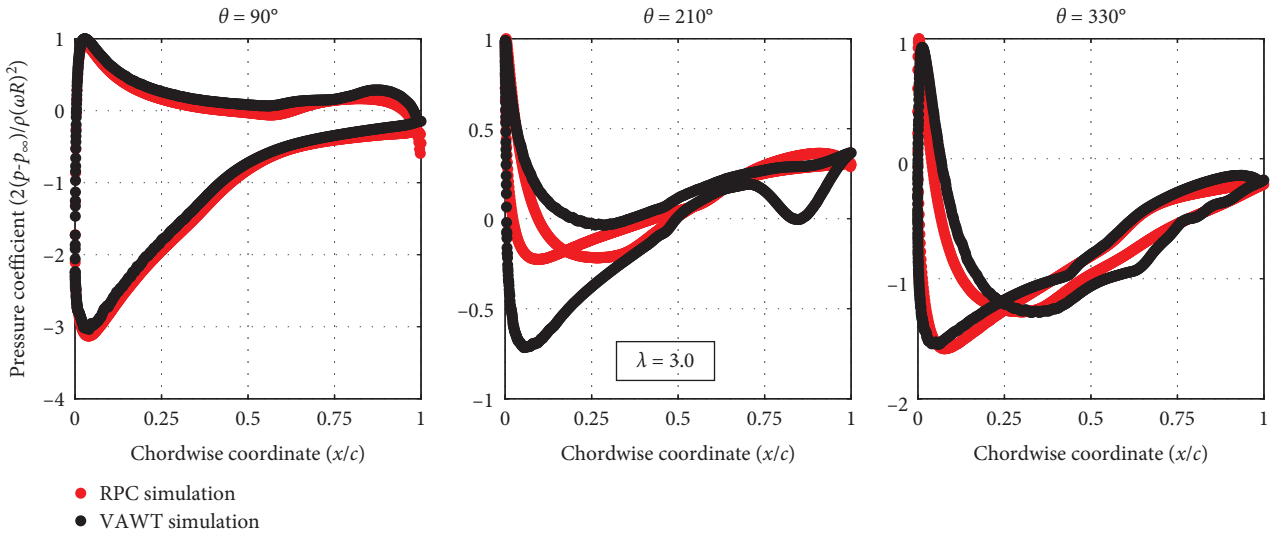

FIGURE 12: Pressure coefficients over the blades at medium TSR, $\lambda = 3.0$, for azimuthal positions 90°, 210°, and 330°. Comparison between the results for a conventional 2D URANS three-bladed simulation (VAWT) and the rotating pitching approach (RPC).

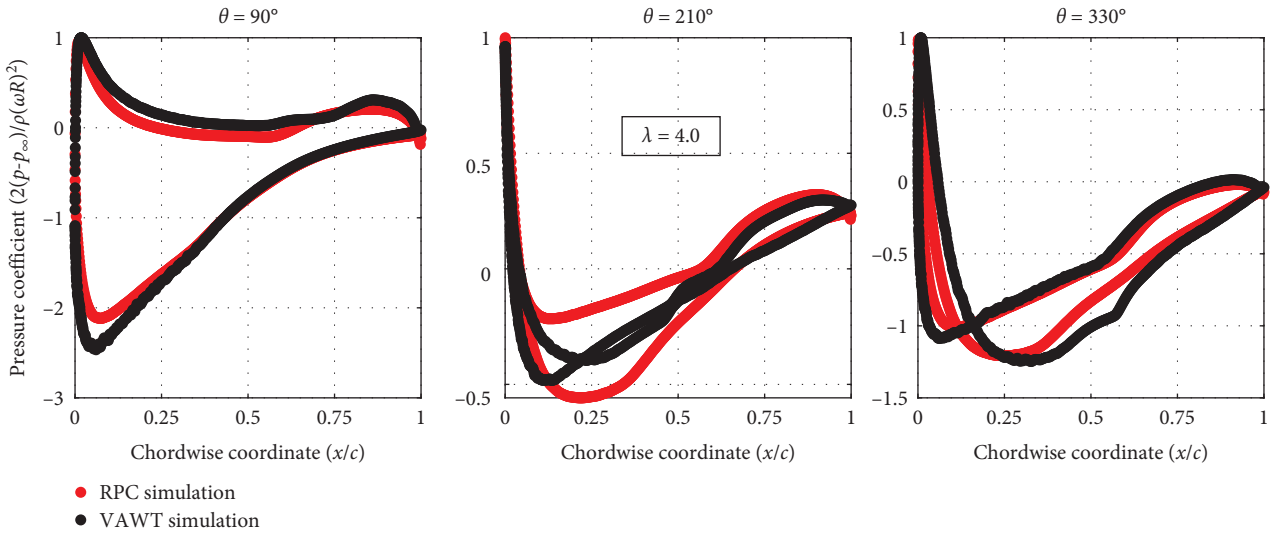

FIGURE 13: Pressure coefficients over the blades at high TSR, $\lambda = 4.0$, for azimuthal positions 90°, 210°, and 330°. Comparison between the results for a conventional 2D URANS three-bladed simulation (VAWT) and the rotating pitching approach (RPC).

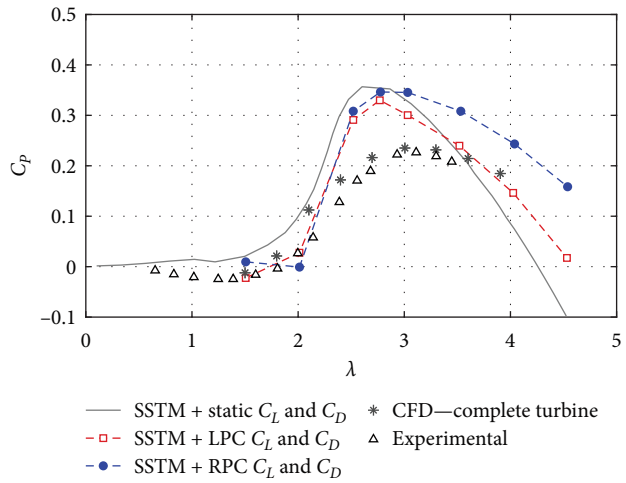

FIGURE 14: Comparison of the performance curve for the VAWT prototype using SSTM model under different input data for the aerodynamic coefficients.

model employed used a single value of the induction factor for all the azimuthal positions of the blade motion under equivalent pitching conditions. The implementation of more sophisticated analytical models for the whole procedure, like the MSTM or—even better—the DSTM, is expected to improve further the agreement with the experiments. Finally, note that although unmixed wakes were found to play a relevant role in the prediction of blade forces at low TSR values (in terms of pressure coefficients), their contribution to the overall performance is revealed nonsignificant in the C_p–λ curve (see the overlapping of pitching curves and experimental markers up to TSR = 2.0).

The RPC methodology combined with analytical models has been proven to be a useful, time-saving, and computationally economic option to estimate the performance of any VAWT design. Furthermore, the resolution of the flow around the blades under pitching motion using the rotating cascade resembles with high fidelity the flow patterns of the real turbine.

To illustrate this fact, Figure 15 exhibits the wake vorticity maps for the airfoil under rotating pitch motion for several blade positions, corresponding to 90° up to 210° of azimuthal angle, in the case of low TSRs ($\lambda = 2.0$). For a better representation, the colormap for the vorticity field is logarithmically scaled. These angles have been selected because they correspond to the most adverse aerodynamical conditions for the blades. Note how the flow is fully detached for the inward side of the blade between 120° and 160°. Massive separation at low shedding frequency characterizes the leeward positions of the airfoil, with the maximum AoA being produced at 115°. Despite of the progressive decreasing in the AoA, the flow is not fully recovered until going up to 180° when the AoA becomes negative. In addition, also at 180° the Reynolds number on the airfoil is the lowest one (Table 6), which severely penalizes the aerodynamics of the airfoil.

Similarly, Figure 16 presents the results for medium TSRs ($\lambda = 3.0$). It is evident that no full-detached conditions are

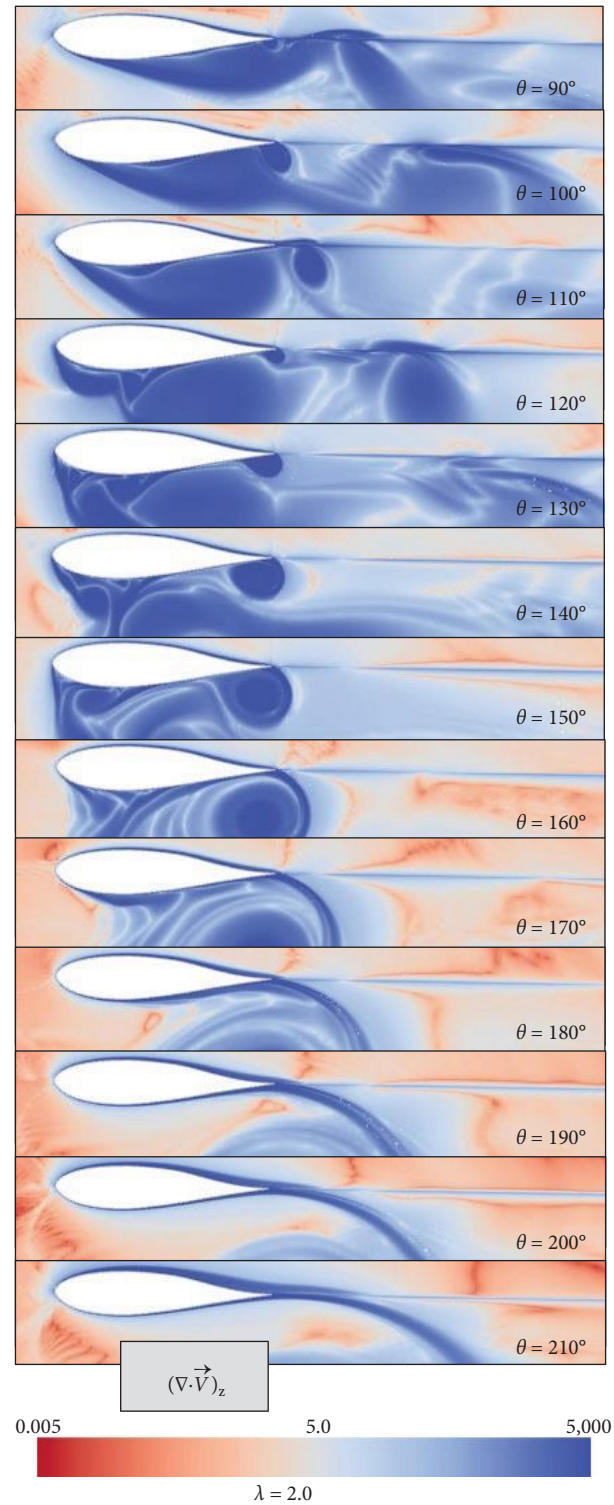

FIGURE 15: Vorticity maps over the rotating pitching airfoil for tip-speed ratio of $\lambda = 2.0$ (angular positions from 90° to 210°).

met at any of the positions shown in the figure. However, from midchord to the trailing edge of the inward side of the blade, flow separation occurs practically at all azimuthal angles. Note how the frequency of the vortex shedding is increased, with the associated reduction in the amplitude

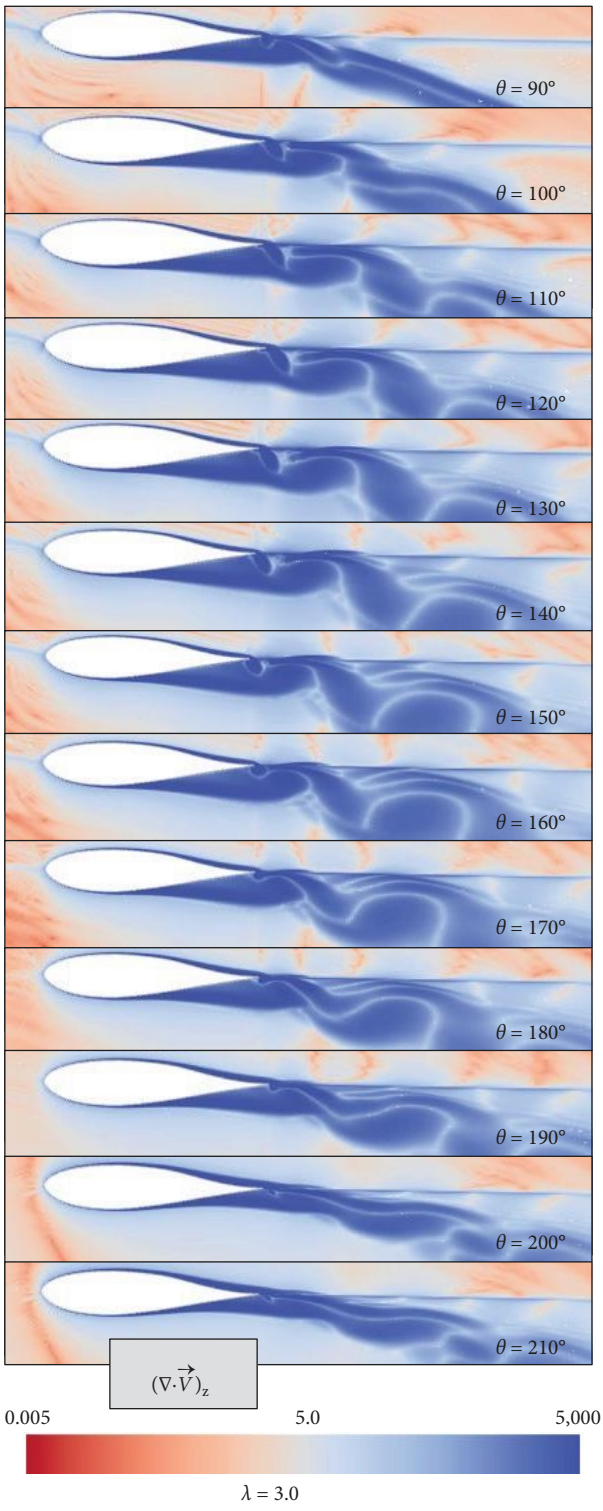

FIGURE 16: Vorticity maps over the rotating pitching airfoil for tip-speed ratio of $\lambda = 3.0$ (angular positions from 90° to 210°).

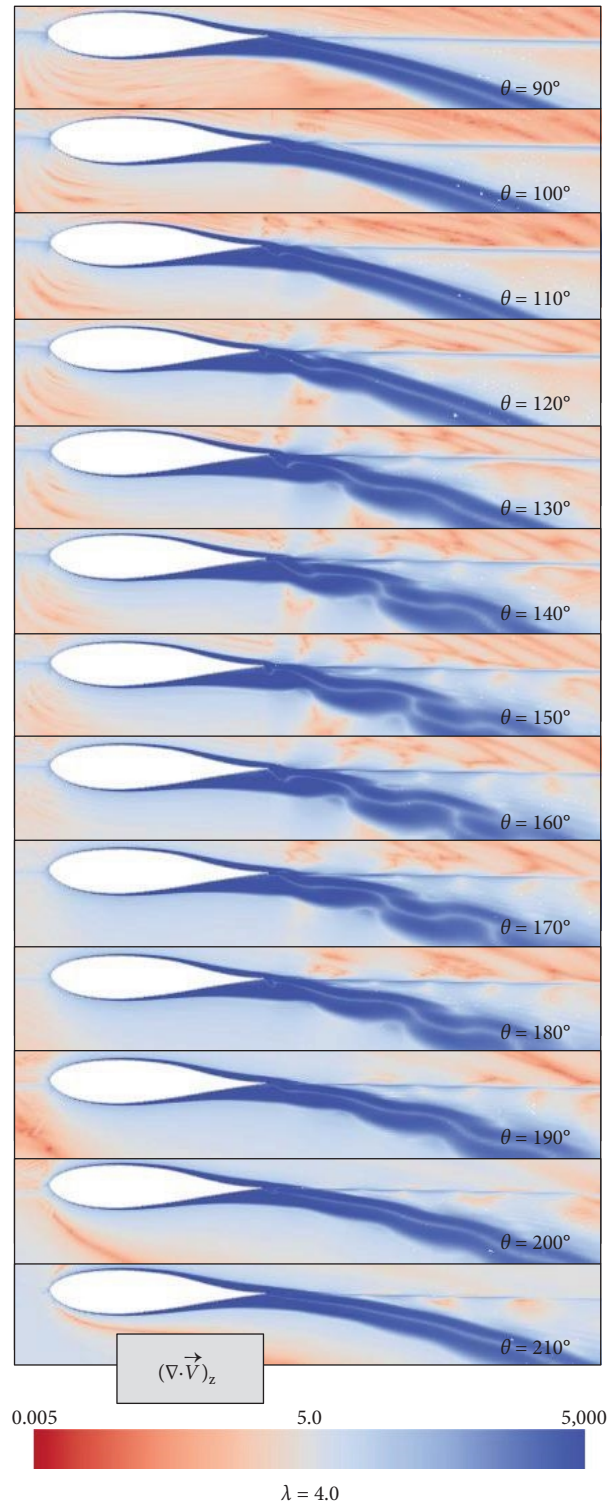

FIGURE 17: Vorticity maps over the rotating pitching airfoil for tip-speed ratio of $\lambda = 4.0$ (angular positions from 90° to 210°).

of the oscillations. Note also that the variation of the Reynolds number shown for all the positions is clearly more favorable than in the previous TSR.

Finally, Figure 17 provides the evolution of the vorticity maps at high TSRs ($\lambda = 4.0$). The difference in wake convection for this high operating condition is clearly observed with respect to previous situations. Only between 120° and 190°, a slight separation of the flow at the trailing edge is revealed, mainly produced by the instable engrossment of the boundary layer at the inward side of the blade. Even in this case at high

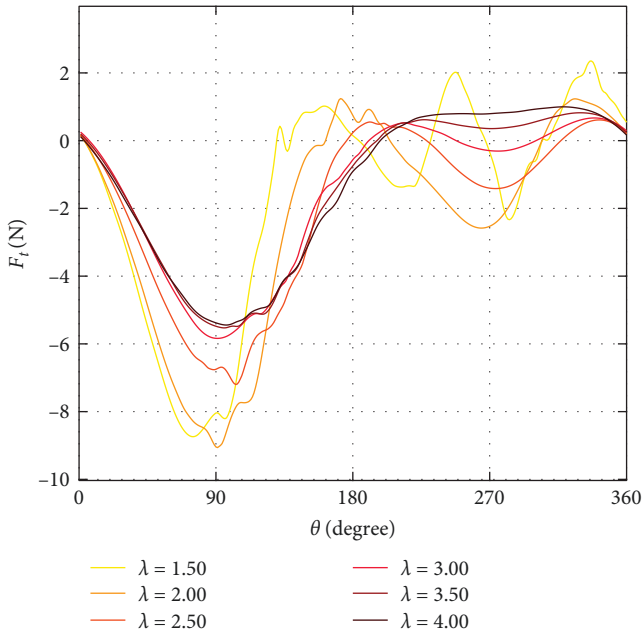

FIGURE 18: Evolution of the tangential force on the airfoil as a function of the TSR for one full cycle of the rotating pitching motion.

TSR, independency from the Reynolds number is still not guaranteed (around 150,000 for this DU airfoil) in these compromised angular positions.

It is interesting to assess how those unstable variations of the flow structures over the blades are conditioning the instantaneous values of the tangential force (responsible for the turbine torque). For that purpose, Figure 18 presents the evolution of the horizontal force on the blade obtained from the results of all the cases simulated using the rotating pitch cascade. Note that in the pitching simulation, the horizontal (chordwise) direction, coincident with the x-coordinate of the blade, mimics the tangential coordinate of the blade in the VAWT environment. Due to the sign convention selected, negative values of tangential force correspond to positive torque generation. Since the maximum power is attained at TSR values around 3.0, the red curve in Figure 18 provides the reference torque output of this operating point. At higher TSRs, the curves tend to collapse in the region for positive angles of attack (between 0° and 180°), presenting notable differences in the windward region (from 210° to roughly 360°). At low and very low TSRs, positive torques in the windward region from 0° to 180° are more pronounced, but rapidly diminishing because of the massive separations illustrated earlier.

It deserves to pay attention that the integration, over one full cycle, of these tangential forces exerted on the airfoil during the simulation directly provides the mean force responsible for the aerodynamic torque and thus the output power of the turbine. Hence, not only the performance curve of the turbine can be obtained by means of the application of previous analytical models with pitching coefficients but also can be obtained from the mean value of the chordwise force over the pitching blade under rotating cascade, further multiplied by the turbine radius, the number of blades and the rotational speed for the TSR condition under study. However, since the SSMT model employed here introduces one unique value of the induction factor for all the azimuthal angles of the blade, the computed tangential forces are not fully representative of the real torque expected from the turbine. Analytical models with multiple tubes, and even with a double disk arrangement to consider upwind and downwind domains of the turbine, may improve the temporal description of the tangential forces, thus validating this technique to estimate the turbine performance curve.

4. Conclusions

A 2D-URANS CFD model, with k-ω SST turbulence model and UDF functionalities of a DU-06-W-200 airfoil, employed in an H-rotor VAWT prototype, has been simulated under equivalent unsteady pitching conditions to retrieve the performance curve of the three-bladed full machine. Two different approaches have been explored, linear pitching cascade (LPC) and rotating pitching cascade (RPC). The frequencies and amplitudes of the pitching motion have been adjusted to represent the operational range of tip-speed ratios (TSRs) for the wind turbine. The potential flow effects have been introduced by calculating suitable induction factors using a simple stream tube model (SSTM) through an iterative process. A comprehensive comparison has been performed to evaluate the accuracy and efficiency of the pitching methodology, including results of a SSTM with static coefficients, a 2D-URANS CFD of the whole turbine with sliding mesh, and wind tunnel tests of a scaled prototype of the turbine. Flow variables as pressure distribution over the blades and vorticity maps have been compared with the whole complete CFD.

Both linear and rotating pitching aerodynamic coefficients notably improve the output of analytical models with respect to static coefficients. Although their performance curves overlap in low-to-medium TSRs, linear pitching produces worse results in higher TSRs due to the increased relevance of the inherent curvature of the wake. Considering that the rotating approach of the pitching cascade does not need additional computational effort, it is posed as the preferred methodology.

Furthermore, it has been demonstrated that it is able to predict reasonable estimations with remarkable numerical economy compared with a conventional CFD of the whole turbine. Particularly, the TSR of the maximum performance coefficient is accurately predicted, though its magnitude is still overestimated because of the nonconsidered 3D effects and the simplicity of the analytical model. Additionally, the effect of adjacent wakes produced by upwind airfoils could also be related to the overestimation found in the results.

The comparison of the pressure distributions and vorticity maps between the rotating pitching simulation and the whole turbine simulation showed significant differences for low TSRs, despite the accurate estimation of the performance coefficient in this range. Nevertheless, for medium-to-high TSRs, a remarkable match was revealed, demonstrating the utility of RPC to study flow characteristics.

Further efforts must be considered to improve the predictions of the pitching procedure. In particular, it is expected that using a double-disk, multiple-tube DSTM model may boost the results from the pitching simulations. This would have a double effect; in the CFD modeling due to the inclusion of a more realistic induction factor that fully considers the azimuthal position of the blades and the windward and leeward regions of the turbine, and in the estimation of the curve because of the less simplifications considered in the analytical model.

Data Availability

The data that support the findings of this study are available from the corresponding author upon reasonable request.

Conflicts of Interest

The authors declare that they have no conflicts of interest.

Acknowledgments

This research was funded by the Agencia Estatal de Investigación (AEI) of the Spanish Ministry of Science and Innovation, in the context of the State Program to Promote Scientific–Technical Research and its Transfer, through the Project "Optimization through flow control techniques of a vertical axis wind turbine for urban environments," included in the Next Generation EU funds of the European Community (TED2021-131307B-I00).

References

[1] B. Hand and A. Cashman, "A review on the historical development of the lift-type vertical axis wind turbine: from onshore to offshore floating application," *Sustainable Energy Technologies and Assessments*, vol. 38, Article ID 100646, 2020.

[2] R. Kumar, K. Raahemifar, and A. S. Fung, "A critical review of vertical axis wind turbines for urban applications," *Renewable and Sustainable Energy Reviews*, vol. 89, pp. 281–291, 2018.

[3] F. Balduzzi, A. Bianchini, E. A. Carnevale, L. Ferrari, and S. Magnani, "Feasibility analysis of a Darrieus vertical axis wind turbine installation in the rooftop of a building," *Applied Energy*, vol. 97, pp. 921–929, 2012.

[4] M. Borg and M. Collu, "A comparison between the dynamics of horizontal and vertical axis offshore floating wind turbines," *Philosophical Transactions of the Royal Society A: Mathematical, Physical and Engineering Sciences*, vol. 373, no. 2035, p. 20140076, 2015.

[5] S. H. Hezaveh, E. Bou-Zeid, J. Dabiri, M. Kinzel, G. Cortina, and L. Martinelli, "Increasing the power production of vertical-axis wind-turbine farms using synergistic clustering," *Boundary-Layer Meteorology*, vol. 169, no. 2, pp. 275–296, 2018.

[6] A. Rezaeiha, H. Montazeri, and B. Blocken, "Towards accurate CFD simulations of vertical axis wind turbines at different tip speed ratios and solidities: guidelines for azimuthal increment, domain size and convergence," *Energy Conversion and Management*, vol. 156, pp. 301–316, 2018.

[7] A. Meana-Fernández, I. Solís-Gallego, J. M. Fernández Oro, K. M. Argüelles Díaz, and S. Velarde-Suárez, "Parametrical evaluation of the aerodynamic performance of vertical axis wind turbines for the proposal of optimized designs," *Energy*, vol. 147, pp. 504–517, 2018.

[8] L. Santamaría, J. A. M. Fernández Oro, K. M. D. Argüelles Díaz, A. Meana-Fernández, B. Pereiras, and S. Velarde-Suárez, "Novel methodology for performance characterization of vertical axis wind turbines (VAWT) prototypes through active driving mode." *Energy Conversion and Management*, vol. 258, Article ID 115530, 2022.

[9] B. Hand, G. Kelly, and A. Cashman, "Aerodynamic design and performance parameters of a lift-type vertical axis wind turbine: a comprehensive review," *Renewable and Sustainable Energy Reviews*, vol. 139, Article ID 110699, 2021.

[10] H. Jeong, S. Lee, and S.-D. Kwon, "Blockage corrections for wind tunnel tests conducted on a Darrieus wind turbine," *Journal of Wind Engineering and Industrial Aerodynamics*, vol. 179, pp. 229–239, 2018.

[11] D. B. Araya and J. O. Dabiri, "A comparison of wake measurements in motor-driven and flow-driven turbine experiments," *Experiments in Fluids*, vol. 56, no. 7, Article ID 150, 2015.

[12] R. Howell, N. Qin, J. Edwards, and N. Durrani, "Wind tunnel and numerical study of a small vertical axis wind turbine," *Renewable Energy*, vol. 35, no. 2, pp. 412–422, 2010.

[13] B. Dou, Z. Yang, M. Guala, T. Qu, L. Lei, and P. Zeng, "Comparison of different driving modes for the wind turbine wake in wind tunnels," *Energies*, vol. 13, no. 8, Article ID 1915, 2020.

[14] I. Paraschivoiu, "Wind turbine design: with emphasis on darrieus concept," 2002.

[15] L. Santamaría, M. G. Vega, A. Pandal, J. González Pérez, S. Velarde-Suárez, and J. A. M. Fernández Oro, "Aerodynamic performance of VAWT airfoils: comparison between wind tunnel testing using a new three-component strain gauge balance and CFD modelling," *Energies*, vol. 15, no. 24, Article ID 9351, 2022.

[16] P. R. Spalart and S. R. Allmaras, "A one-equation turbulence model for aerodynamic flows," *La Recherche Aérospatiale*, vol. 1, pp. 5–21, 1994.

[17] F. Menter, R. Sechner, A. A. Matyushenko, and S. Petersburg, "Best practice: RANS turbulence modeling in Ansys CFD," 2019, https://fluidcodes.ir/rans-turbulence-modeling/.

[18] F. R. Menter, A. Matyushenko, and R. Lechner, "Development of a generalized K-ω two-equation turbulence model," *Notes on Numerical Fluid Mechanics and Multidisciplinary Design*, vol. 142, pp. 101–109, 2020.

[19] A. Sanvito, V. Dossena, and G. Persico, "Formulation, validation and application of a novel 3D BEM tool for vertical axis wind turbines of general shape and size," *Applied Sciences*, vol. 11, no. 13, Article ID 5874, 2021.